RSC Advances

PAPER

View Article Online
View Journal | View Issue

Cite this: *RSC Adv.*, 2016, **6**, 32037

Martensitic transition, spin glass behavior and enhanced exchange bias in Si substituted $Ni_{50}Mn_{36}Sn_{14}$ Heusler alloys†

G. R. Raji,[a] Bhagya Uthaman,[a] Rajesh Kumar Rajan,[a] Sharannia M. P.,[b] Senoy Thomas,[a] K. G. Suresh[c] and Manoj Raama Varma*[a]

Received 18th January 2016
Accepted 21st March 2016

DOI: 10.1039/c6ra01484d

www.rsc.org/advances

The martensitic transition and exchange bias properties of the Heusler alloy system $Ni_{50}Mn_{36}Sn_{14-x}Si_x$ (x = 0, 1, 2 and 3) have been investigated. As the Si concentration increases, the martensitic transition temperature decreases while the Curie temperature of the austenite phases shows a slight increase. The temperature dependence of AC susceptibility with different frequencies at a low temperature regime was analyzed and the frequency dependence of the spin freezing temperature (T_f) showing a conventional critical slowing down relation confirms the spin glass behavior at low temperatures. Furthermore, the sample was recognized as a reentrant spin glass with both ferromagnetic and glassy states coexisting at least in the field cooled state. Due to these competing magnetic interactions, all the studied alloys exhibit exchange bias at low temperatures. For x = 2 alloy, an exchange bias field of 235 Oe is observed. However, on further increasing x, the exchange bias decreases. Therefore, it is quite evident that the unidirectional anisotropy decreases as a function of Si concentration. The double shifted hysteresis loop after zero field cooling and training effect strongly support the presence of exchange bias in these alloys. The dependencies of EB on various parameters like temperature and cooling field have also been investigated.

I. Introduction

Ferromagnetic shape memory materials are in the limelight today due to their various properties, one of which is exchange bias (EB). The EB effect was discovered by Meiklejohn and Bean in Co/CoO nanoparticles at low temperatures in 1956, where they observed a shift in the hysteresis loop along the magnetic field axis.[1] Substantial investigations have been carried out in oxide particles, multilayer films and nonhomogeneous materials[2–8] due to the application of EB in ultrahigh-density magnetic recording, giant magnetoresistance sensors, and spintronic devices *etc.* It refers to the directional shift in the hysteresis loop of a ferromagnet (FM) in contact with an antiferromagnet (AFM), when the sample is cooled in an external field to below the Néel temperature (T_N) of the antiferromagnet. Generally, the exchange anisotropy results from the coupling between the FM and AFM layers at the interface, which gives a shift in the hysteresis loop along the field axis.

Recently, Ni–Mn–X (X = In, Sb, Sn) Heusler alloys which show shape memory effect and magnetism simultaneously, have drawn much attention due to some interesting properties, such as magnetic-field-induced strain, magnetoresistance, magnetocaloric effect and exchange bias properties.[9–13] In Ni–Mn–X alloys, after the martensitic transition, the Mn–Mn distance would decrease due to the twinning of the martensitic phase, leading to the enhanced strength of the antiferromagnetic exchange coupling.[14] It is well known that magnetic properties of the above said Heusler alloys are strongly dependent on Mn content and Mn–Mn distance between different lattice sites. The coexistence of FM and AFM phases in the martensitic phase and the coupling at the FM/AFM interface would result in EB behavior, which has been observed in $Ni_{50-x}Co_xMn_{38}Sb_{12}$,[15] $Ni_{50}Mn_{36}Sn_{14-x}Ge_x$ (x = 1, 2),[16] $Mn_{50}Ni_{42}Sn_8$,[17] $Ni_{50}Mn_{35}In_{15}$,[18] $Mn_{50}Ni_{40}Sn_{10}$ [19] alloys, *etc.* Furthermore, coexistence of spin glass-like state and FM has been reported in certain alloys of this family.[20,21] In the present work, we have studied the effect of Si doping at Sn site on structural, magnetic and exchange bias properties of $Ni_{50}Mn_{36}Sn_{14}$ alloys.

II. Materials and methods

Polycrystalline ingots of $Ni_{50}Mn_{36}Sn_{14-x}Si_x$ (x = 0, 1, 2 and 3) were prepared by arc melting the stoichiometric amounts of Ni, Mn, Sn and Si of at least 99.99% purity in high pure argon

[a]*Materials Science and Technology Division, National Institute for Interdisciplinary Science and Technology, CSIR-NIIST, Thiruvananthapuram-695 019, India. E-mail: manojraamavarma@yahoo.co.uk; manoj@niist.res.in*

[b]*Department of Physics, Indian Institute of Technology, 600036, Chennai, India*

[c]*Department of Physics, Indian Institute of Technology, 400076, Mumbai, India*

† Electronic supplementary information (ESI) available. See DOI: 10.1039/c6ra01484d

atmosphere. After that, the samples were sealed in evacuated quartz tubes and annealed at 950 °C for 48 h. The samples annealed were subsequently quenched in ice water mixture. Annealed samples were ground well and subjected to powder X-ray diffraction (XRD) analysis using high resolution Rigaku SmartLab XRD diffractometer with step size 0.02° in Bragg–Brentano geometry with Cu-Kα radiation in the 2θ range of 20° to 80°. The phase purity and crystal structure of all the compositions were confirmed from Rietveld refinement of the XRD data using the EXPGUI software and the cubic $L2_1$ structures of the samples were established. The elemental compositions were determined by using a scanning electron microscope (SEM) equipped (Carl Zeiss Evo 18) with an energy dispersive X-ray spectrometer (Oxford EDAX X-Max^N) and are summarized in Table 1. The HRTEM images were taken using transmission electron microscopy (TEM, FEI Tecnai G230S Twin 300 kV). Magnetization measurements were performed by using a Physical Property Measurement System [Quantum Design, Dynacool].

III. Results and discussion

A. Structural analysis

The Rietveld refined room temperature powder XRD patterns for the $Ni_{50}Mn_{36}Sn_{14-x}Si_x$ ($x = 0$, 1, 2 and 3) alloys are depicted in Fig. 1. The samples are in the cubic austenite phase and have a Heusler $L2_1$ structure with the space group $Fm\bar{3}m$.[14,16] In the room temperature austenite phase of the X_2YZ full Heusler alloy, 'X' occupies the (1/4, 1/4, 1/4) site, Y at (0, 0, 0) site and Z at (1/2, 1/2, 1/2) site. In the present system, Ni occupies the X site, Mn occupies the Y site and the extra Mn (36–25) along with Sn and doped Si occupies the Z site. In addition to the ordered $L2_1$ structure, generally several types of disordered structures have been observed in Heusler alloys. In the case of $L2_1$ structure, when the Y and Z atoms replace their sites and eventually occupy their sites absolutely at random, the compound transforms into commonly observed disordered B2 structure (Y and Z sites become equivalent). At high temperatures X, Y and Z atoms distributes randomly, *i.e.* complete disorder in the X_2YZ Heusler compounds, results in the A2 structure-type with reduced symmetry. As a result, the X, Y and Z sites become equivalent leading to a BCC lattice. A disorder–order transition A2 → B2 → $L2_1$ has been reported in most of the Heusler alloy systems. Most of these alloys are predominantly in a cubic $L2_1$ structure near room temperature, which is called austenite phase. By decreasing the temperature it transfers from high symmetry austenite to a very complicated low symmetry martensite phase, may be orthorhombic or tetragonal.[15,21]

From the XRD patterns, it is clear that (220) peak shifts slightly towards higher angles with increase in Si content, which indicates a decrease in lattice volume due to the smaller size of Si as compared to that of Sn. The lattice parameters are found to be $a = 5.99$ Å, 5.97 Å, 5.96 Å and 5.94 Å for $x = 0$, 1, 2 and 3 respectively obtained from the refined data are depicted in Table 2. Variations of fit parameters R_{wp} and R_p with silicon composition are also shown in Table 2. For $x = 3$ composition, R_{wp} is large when compared with other compositions. This may be due to the poor fitting of the experimental data with the reference data (ordered $L2_1$). But a systematic trend in the variation of R_{wp} is not observed.

Fig. 2 shows the HRTEM images acquired from sample $Ni_{50}Mn_{36}Sn_{11}Si_3$. In high resolution, the planes (110), (200) and (220) are clearly seen for the composition $Ni_{50}Mn_{36}Sn_{11}Si_3$. Interplanar spacing ($d$) of these planes measured from the TEM images match with the calculated values of corresponding planes for the Heusler alloys with $L2_1$ phase. Typical SAED pattern recorded shows a spotty nature. The d values corresponding to these spots are indexed as shown in Fig. 2(b).

Table 1 Compositions of $Ni_{50}Mn_{36}Sn_{14-x}Si_x$ ($x = 0$, 1, 2 and 3) determined by EDAX analysis. The estimated error in determining the concentration of each element is ±0.1 at%

x (nominal)	Ni at%	Mn at%	Sn at%	Si at%
0	49.63	35.91	14.46	—
1	49.56	35.88	13.29	1.27
2	49.71	36.01	12.21	2.07
3	49.69	35.74	11.43	3.14

B. Magnetic characterization

Fig. 3(a) shows the temperature dependence of magnetization of $Ni_{50}Mn_{36}Sn_{14-x}Si_x$ ($x = 1$, 2 and 3) in an external magnetic field of 500 Oe. Data have been taken in zero-field-cooled (ZFC) and field-cooled cooling (FC) conditions. With decreasing temperature, the paramagnetic–ferromagnetic transition occurs at the Curie temperature of the austenite, T_C^A. With further cooling, the alloys undergo a transition from the ferromagnetic austenite to the martensite phase. The observed thermal hysteresis is attributed to the first-order structural transition. Below this transition, a splitting between the ZFC and FC data is seen at low temperatures, which reveals a low temperature magnetic structure consisting of competing magnetic interactions.

It is observed that an increase in the Si concentration results in a decrease in the martensitic transition temperature (T_M) [see Table 2] which is contrary to the previous reports.[22,23] Generally, the variation of T_M is correlated with the valence electron concentration e/a (electrons per atom), inter atomic distance, strain *etc.*[24] It was reported that in many alloys with increasing e/a value, the martensitic transition temperature also increases.[25] In the present case, the substitution of Si for Sn does not vary the valence electron number but reduces the cell volume. In Ni–Mn–In alloys, it was recently reported that the application of hydrostatic pressure results in an increase of martensitic transition temperature because of the reduction in cell volume.[26] But in our system, the decrease in cell volume with Si substitution produces the opposite effect. The effect of Si substitution for Sn on the martensitic transition temperatures can be explained by using the degree of crystallographic order. In CuZnAl alloy, it was reported that the addition of a fourth element results in the increase of martensitic transition temperature with increasing order of the parent phase.[27] The parent $Ni_{50}Mn_{36}Sn_{14}$ is an

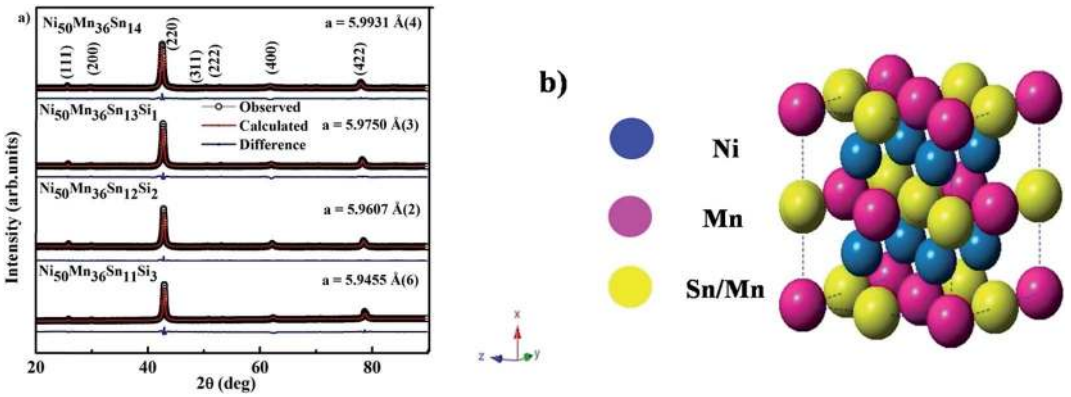

Fig. 1 (a) XRD patterns of $Ni_{50}Mn_{36}Sn_{14-x}Si_x$ ($x = 0$, 1, 2 and 3) at room temperature (b) a crystallographic unit cell description of $Ni_{50}Mn_{36}Sn_{14}$ Heusler alloy.

Table 2 Space group, lattice parameter, atomic volume, R_{wp} (%) and R_p (%) of $Ni_{50}Mn_{36}Sn_{14-x}Si_x$ ($x = 0$, 1, 2 and 3) Heusler alloys

Composition (x)	Space group	Lattice parameter a (Å)	Atomic volume (Å^3)	R_{wp} (%)	R_p (%)
0	$Fm\bar{3}m$	5.9931 (4)	215.253 (4)	2.49	1.56
1	$Fm\bar{3}m$	5.9750 (3)	213.311 (3)	2.34	1.43
2	$Fm\bar{3}m$	5.9607 (2)	211.783 (2)	1.73	1.04
3	$Fm\bar{3}m$	5.9455 (6)	210.167 (6)	3.77	2.65

ordered Heusler-type intermetallic compound with $L2_1$ structure and with the increase in Si concentration, the degree of order decreases. From the original XRD plots, it was estimated that intensities of (111) superlattice peaks decrease (from 19 to 16% relative to (220) peak), which confirms that the degree of order decreases as Si concentration increases from $x = 0$ to 3. Hence the martensitic transition temperature decreases with increase in x (0, 1, 2 and 3).[28]

According to the accepted crystallographic theories, the shear energy is closely related to the mechanical strength of the parent phase.[29,30] With an increase in the strength of the parent phase, the shear energy increases. This warrants more driving force for the initiation of martensitic transition, which results in a decrease of the T_M. It has been reported that in $Ni_{55.5}Fe_{18}Ga_{26.5-x}Si_x$ ($x = 0$, 1 and 2),[30] $Ni_{48}Mn_{39}In_{13-x}Si_x$ ($x = 1$, 2 and 3) ribbons,[31] $Ni_{48}Mn_{39}Sn_{13-x}Si_x$ ($x = 1$, 2, 3 and 4)[28] and $Ni_{50}Mn_{35}In_{15-x}Si_x$ ($x = 1$–5)[32] alloy systems, the substitution of Si leads to a decrease in T_M. However, in $Ni_{43}Mn_{46}Sn_{11-x}Si_x$ ($x = 1$, 2, 3)[22] alloys, T_M increases with increase in Si concentration. Hence in the present investigation, it is reasonable to assume that the increase in strength of the parent alloy due to Si substitution or the degree of crystallographic disorder are the dominating factors than the decrease in cell volume in determining the T_M of the present alloys. The characteristic temperatures of structure transition A_s (austenite start), A_f (austenite finish), M_s (martensite start), M_f (martensite finish) and T_C^A (Curie temperature of the austenite phase), are determined from M–T curves and listed in Table 3.

The presence of antiferromagnetic component in the martensitic phase is supported by the sharp decrease in magnetization associated with the first order austenite–martensite transition. EXAFS study by Bhobe *et al.* on the parent alloy has shown that the Mn–Mn distance between the Mn atoms occupying the Mn and Sn sublattices decreases during martensitic transition, thereby introducing partial AFM in the

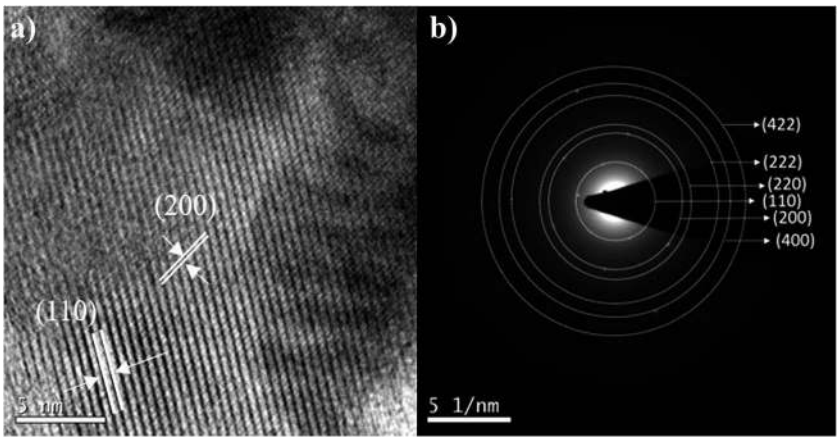

Fig. 2 HRTEM images of (a) $Ni_{50}Mn_{36}Sn_{11}Si_3$ and (b) SAED pattern of $Ni_{50}Mn_{36}Sn_{11}Si_3$ (circles are a guide to eye).

FM matrix.[33] The exchange bias blocking temperature (T_B) can be identified from the zero field cooled $M(T)$ curve [Fig. 3(b)] in the low temperature region. With increasing measuring field [Fig. 4] the characteristic temperatures (A_s, A_f, M_s, M_f and T_M) decreases, and the signature of low temperature magnetic frustration in the ZFC curves disappears, which is a clear indication of the suppression of frozen state at strong magnetic fields.

C. AC magnetic susceptibility measurements

A dynamic study by AC susceptibility measurements have been performed at different frequencies (f) ranging from 433 Hz to 9984 Hz with an AC magnetic field of 1 Oe to understand the nature of low temperature frustrated magnetic state. Fig. 5 shows the temperature dependence of imaginary part (χ'') of the AC susceptibility for $x = 1$ composition at different frequency (f) values. Since the magnetization *versus* temperature curves show identical behavior for all the compositions in the low temperature region, we have presented the AC susceptibility data for $x = 1$, as a representative of the series. The AC susceptibility data are taken in the temperature range 5–250 K, which covers the step like anomaly above T_B in Fig. 3(b). It is interesting to observe that the feature near the step like anomaly is reflected as a small frequency dependant variation on (χ'') values. This is a strong evidence for the proposition of the existence of glassy state at low temperatures. Hence, the shift of χ'' data to higher temperatures with increase in frequency, provide an unambiguous signs of spin slow dynamics in the system.

The frequency dependence of T_f in $\chi''(T)$ can be quantified using the relation $\delta T_f = \Delta T_f/(T_f \Delta \log \omega)$, which is a useful criterion for distinguishing between blocking and freezing processes.[34] The value is typically 0.005 to 0.08 for spin glass (SG) whereas it lies in the range of ~0.1 for non interacting superparamagnetic systems. For the present alloy, the value of δT_f is 0.038 ± 0.002 which lies well within the region corresponding to canonical SG systems.[35,36] This provides yet another strong evidence for the existence of SG behavior in the martensite phase of these alloys.

Table 3 Austenite start (A_s), austenite finish (A_f), martensite start (M_s), martensite finish (M_f), martensitic transition temperature (T_M) and Curie temperature of the austenite phase (T_C^A) obtained for $Ni_{50}Mn_{36}Sn_{14-x}Si_x$ ($x = 0$, 1, 2 and 3)

x	A_s (K)	A_f (K)	M_s (K)	M_f (K)	T_M (K)	T_C^A (K)
0	218	255	238	201	247	316
1	220	254	238	205	246	316
2	187	224	204	166	214	321
3	163	190	177	146	184	326

SG related properties can be further analyzed using critical slowing down relation $\tau/\tau_0 = ((T_f - T_{SG})/T_{SG})^{-z\upsilon}$, where T_{SG}, is the spin glass transition temperature as frequency tends to zero, T_f is the spin freezing temperature, τ is the maximum relaxation time ($\tau = 1/\omega$) corresponding to the measured frequency, τ_0 is the characteristic relaxation time of single spin flip, z is the dynamical critical exponent and, υ is the critical exponent of correlation length, ξ expressed as $\xi = [(T_f/T_{SG}) - 1]^{-\upsilon}$. Fig. 6 shows the variation of $\ln(\tau)$ with the maximum spin freezing temperature (T) with the fitted parameters namely $\tau_0 = (1.49 \pm 0.03) \times 10^{-7}$ s, $T_{SG} = 136.97 \pm 0.02$ K and $z\upsilon = 1.72 \pm 0.07$. Inset of Fig. 6 shows the variation of $\log_{10}\tau$ with $\log_{10}((T_f - T_{SG})/T_{SG})$, which gives a linear dependence with the fitted parameters. For a spin glass system, $\tau_0 \sim 10^{-10}$ to 10^{-13} s and $z\upsilon$ is typically found to lie between 4 and 12, the higher value of τ_0 and lower value of $z\upsilon$ indicates slower spin flipping which is attributed to the presence of randomly oriented ferromagnetic clusters instead of atomic moments. Furthermore, a poor fitting of Arrhenius relation (not shown) suggests that the dynamics of low temperature magnetic state is not merely associated with the single spin flip, but shows a cooperative character. With lowering of temperature, the system first transforms from a paramagnetic to ferromagnetic in nature at $T_C = 316$ K and then from the ordered FM to a disordered glassy phase below T_f. Therefore, the SG phase in our present system is not a conventional spin glass, but a reentrant spin glass [RSG]. A very similar RSG phase and associated EB were also observed in

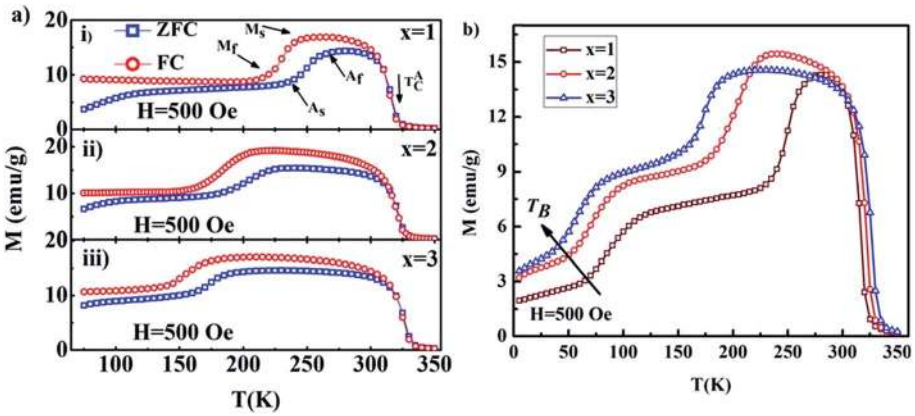

Fig. 3 (a) ZFC and FC magnetization curves for (i) $Ni_{50}Mn_{36}Sn_{13}Si_1$ (ii) $Ni_{50}Mn_{36}Sn_{12}Si_2$ (iii) $Ni_{50}Mn_{36}Sn_{11}Si_3$ at 500 Oe field. (b) Temperature dependence of ZFC magnetization at 500 Oe for $Ni_{50}Mn_{36}Sn_{14-x}Si_x$ ($x = 1$, 2 and 3).

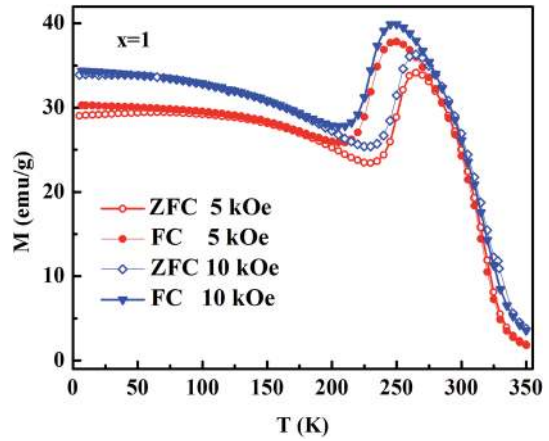

Fig. 4 Temperature dependence of ZFC and FC magnetization measured at 5 kOe and 10 kOe fields for $Ni_{50}Mn_{36}Sn_{13}Si_1$.

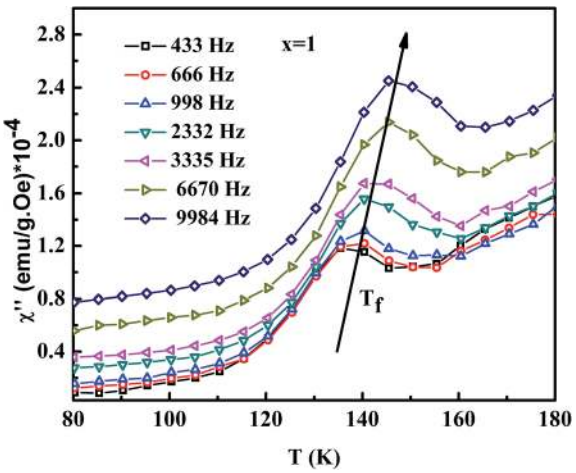

Fig. 5 Temperature dependence of imaginary part (χ'') of the ac susceptibility measured at different applied frequencies with an ac magnetic field of 1 Oe for $x = 1$ alloy.

$Ni_2Mn_{1.36}Sn_{0.64}$ and $Ni_2Mn_{1.44}Sn_{0.56}$ alloys.[35] This prompts us to propose a generic view of the RSG-type magnetic ground state in higher Si doped alloys showing EB, where a common spin freezing phenomena is responsible for the observed exchange bias in these alloys.

D. Exchange bias properties

Fig. 7 shows the isothermal magnetization curves for $Ni_{50}Mn_{36}Sn_{14-x}Si_x$ ($x = 0$, 1, 2 and 3) at different temperatures, after field cooling in a field of 10 kOe from 350 K to the desired measurement temperatures. The isothermal magnetization measurements were performed in the field range of ±20 kOe. For the sake of clarity, we have shown the hysteresis loops only in the field range of ±2 kOe in the figure. Fig. 7(a)–(d) shows the hysteresis loops for $x = 0$, (e)–(h) for $x = 1$, (i)–(l) for $x = 2$ and (m)–(p) for $x = 3$ at different temperatures. It is evident from the figures that the amount of the shift in the hysteresis loop decreases with increase in temperature. The temperature above which the hysteresis loop becomes symmetric, nearly coincides

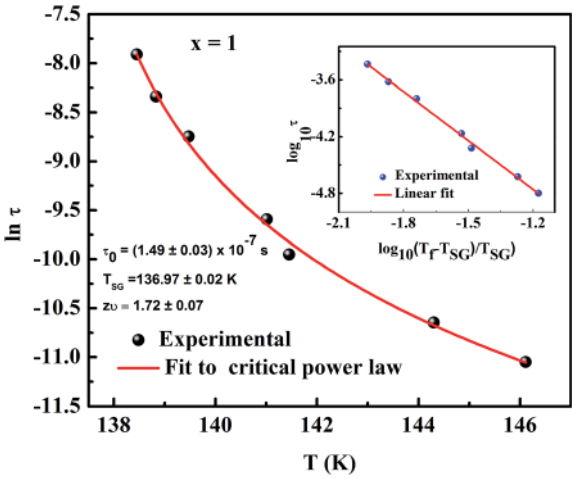

Fig. 6 $\ln(\tau)$ *vs.* maximum spin freezing temperature (T) fitted to the critical power law. Inset shows the variation of $\log_{10}\tau$ with $\log_{10}((T_f - T_{SG})/T_{SG})$ for $x = 1$ alloy. The solid line represents the linear fit to the experimental data.

with the blocking temperature observed from the M–T data shown in Fig. 3(b). The presence of finite shift of the loops is characteristics of exchange bias present in the system, which is attributed to the existence of spin glass like freezing at low temperatures.

All stoichiometric Heusler compositions (Ni_2MnZ) are ferromagnetic with the Curie point above room temperature. The excess Mn doping at the expense of Z atoms induces structural instability in the system leading to the first order martensitic structural transition as shown in the phase diagram.[37] Evidently, the magnetic nature of the ground state of the Ni–Mn–Sn alloys consists of excess Mn atoms occupying the Sn-sites in the lattice. The Mn atoms at regular sites constituted the FM phase and the excess Mn atoms at Sn sites are acting as the AFM phase. The EB was then thought to originate from the AFM exchange interaction between the regular and excess Mn atoms. Therefore, the transition from austenite to the martensite phase leads to the shrinking of the crystallographic axes (a and b), which results in the decrease of the Mn–Mn distances in the lattice and leads to stronger AFM coupling. In the present case, it is expected that FM martensite phase should exist at low temperatures due to the comparatively high M values (in M–T curve). So the magnetic state at low temperatures is very much complex due to the coexistence of FM and AFM exchange interactions, which leads to the magnetic frustration. As discussed earlier, the temperature dependence of AC susceptibility confirms the reentrant spin glass behavior in the present case. Therefore, the EB effect in the system can be attributed to the pinning effect of the FM at SG-like interface, unlike the reports found in some Ni–Mn based magnetic shape memory alloys where EB effect has been suggested to arise from the FM/AFM interfaces.

The ZFC M–H curve of $Ni_{50}Mn_{36}Sn_{12}Si_2$ at 5 K is shown in Fig. 8, which shows a double shifted nature (the middle region of the curve is shown for better clarity). This is a clear indication

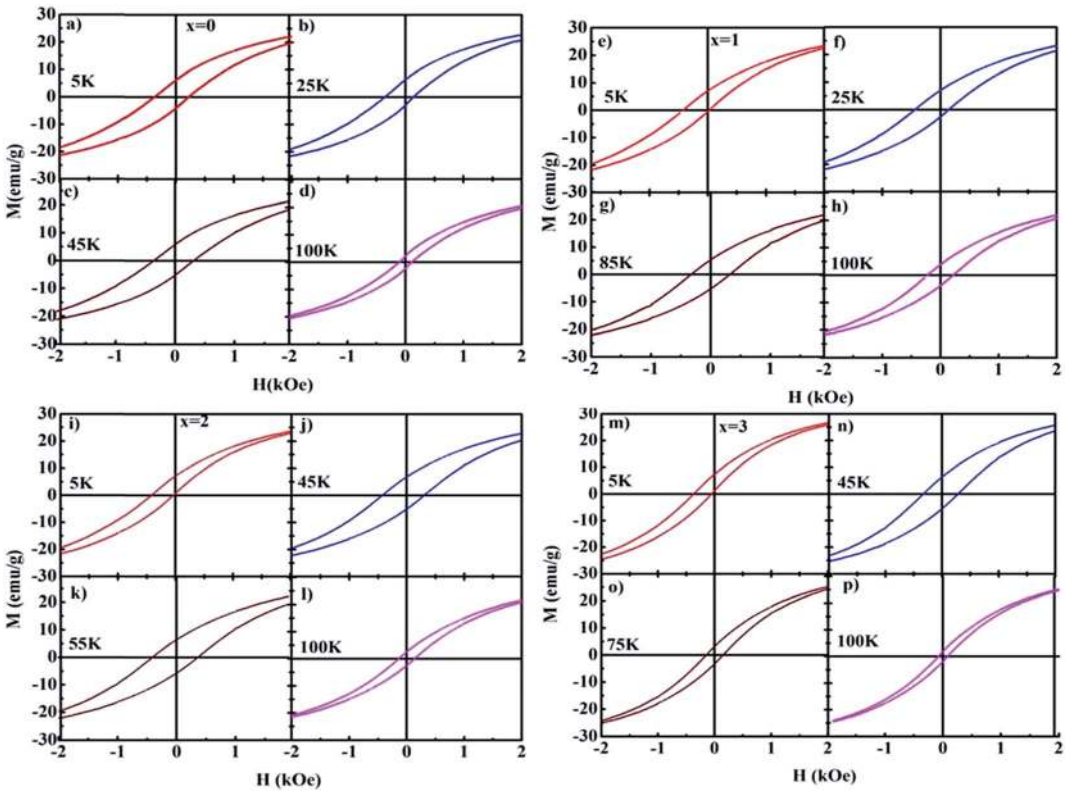

Fig. 7 Magnetic hysteresis loops of alloys $Ni_{50}Mn_{36}Sn_{14-x}Si_x$ ($x = 0$, 1, 2 and 3) measured at different temperatures after field cooling the sample from 350 K in an applied field of 10 kOe.

of the complex state of the martensite phase with magnetic frustration. During the measurement process, the AFM regions couple oppositely with the adjacent ferromagnetic region, giving rise to the double shifted loop, similar to the one seen in well known exchange bias systems.[38] The presence of double shifted ZFC loop and the shifted FC loops are the results of unidirectional anisotropy and exchange bias, both of which arise from the interfacial exchange coupling between the two magnetically different phases at low temperatures.[39]

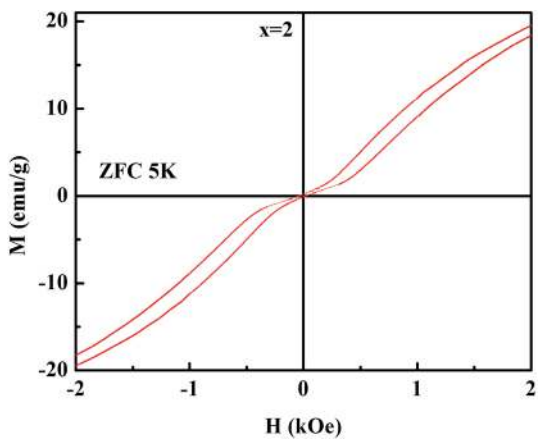

Fig. 8 Magnetic hysteresis loop obtained in the ZFC mode for $Ni_{50}Mn_{36}Sn_{12}Si_2$ at 5 K.

Exchange bias field (H_{EB}) and coercivity (H_C) are calculated using the relations $H_{EB} = -(H_1 + H_2)/2$ and $H_C = |H_1 - H_2|/2$, where H_1 and H_2 are the coercivity at the descending and ascending branch of the M–H loop respectively (note that the error in H_{EB} and H_C determination is ± 0.3 Oe). Another indication of the presence of exchange bias in a system is the enhancement of coercivity (H_C) in the field cooled hysteresis compared to the zero field cooled case. This is due to the development of exchange (unidirectional) anisotropy in the system. The coercivity value determined from FC M–H is greater than the corresponding ZFC M–H curve, at 5 K. The variation of H_C for different compositions under zero field and field cooled conditions at 5 K is depicted in Fig. 9 and all the samples follows the same trend. Also, the value of magnetization at 20 kOe for the field-cooled mode is higher than that of zero field cooled case, due to the increase in ferromagnetic component during FC.

Fig. 10(a) shows the variation of exchange bias field (H_{EB}) and coercivity (H_C) as a function of temperature for $x = 2$. H_{EB} shows an approximately linear decrease with temperature and becomes zero above 90 K. On the other hand, the value of H_C increases initially, reaches a maximum and then decreases with increase in temperature. The exchange bias field at different temperatures for $x = 0$, 1 and 2 are shown in Fig. 10(b). There is an approximately linear decrease of H_{EB} with temperature. As temperature increases, the exchange coupling between the two magnetically different regions decreases and the effect

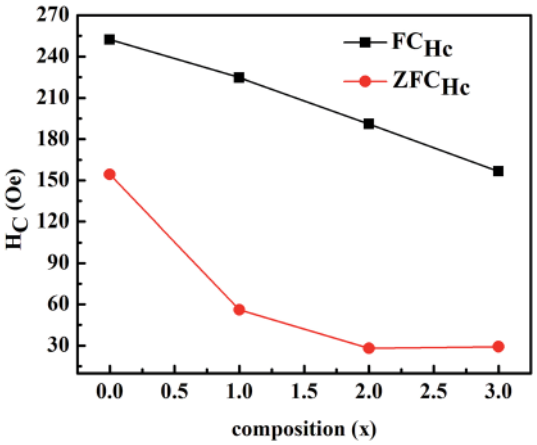

Fig. 9 Variation of H_C for different compositions under zero field and field cooled conditions at 5 K for $Ni_{50}Mn_{36}Sn_{14-x}Si_x$ ($x = 0$, 1, 2 and 3).

disappears beyond the blocking temperature since the spin glass phase is thermally unstable at higher temperatures. The increase of H_C with temperature can also be ascribed to the competition between the interfacial exchange coupling strength and AFM anisotropy.[40,41] Inset in Fig. 10(b) shows the variation of exchange bias field with Si concentration at 5 K, which shows that the H_{EB} increases from 123 Oe to 235 Oe as x is increased from 0 to 2 and thereafter it get decreases. From this, it is quite evident that the unidirectional anisotropy changes as a function of Si concentration.

The cooling field dependence of H_{EB} at 5 K for $Ni_{50}Mn_{36}Sn_{14-x}Si_x$ ($x = 2$) was also investigated. The sample was cooled from 350 K to 5 K in different fields and the magnetic isotherms were measured in ±20 kOe field range. The results are depicted in Fig. 11 and it is found that H_{EB} decreases with cooling field. This is because, as the magnitude of cooling field increases the Zeeman coupling also increases, so that the exchange coupling between the two phases decreases, resulting in a decrease in H_{EB}.[41]

The training effect is one of the important experimental evidences which is usually observed in EB materials, where a decrease of H_{EB} is seen by cycling the system through several hysteresis loops.[2] To confirm whether such an effect is present in our system, we have measured several hysteresis loops at 5 K after field cooling in 50 kOe. The first and the sixth loops are shown for $Ni_{50}Mn_{36}Sn_{12}Si_2$ in Fig. 12 (only the middle region of the curve is shown for better clarity). The decrease in H_{EB} with the number of cycles confirms the presence of training effect in the system. The training effect is interpreted in terms of metastable magnetic disorder at the magnetically frustrated interface during magnetization reversal process. It arises mainly because of the weakening of interfacial exchange coupling as a result of partial loss of the net magnetization of the frustrated layer during repeated field cycling which leads to a drop in the exchange bias. It is generally found that the variation of H_{EB} with n follows the simple power law:[42]

$$H_{EB} - H_{EB\infty} \propto 1/\sqrt{n} \quad (1)$$

where $H_{EB\infty}$ is the EB field in infinite limit of n. The fit of this equation [Fig. 12(b)] shows that the power law matches with the experimental data for the alloy. The value of $H_{EB\infty}$ has been found to be 191 Oe from the fitted curve.

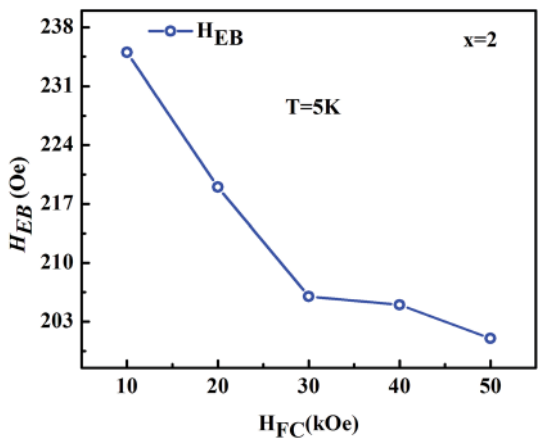

Fig. 11 Variation of H_{EB} with the cooling field for $x = 2$ at 5 K.

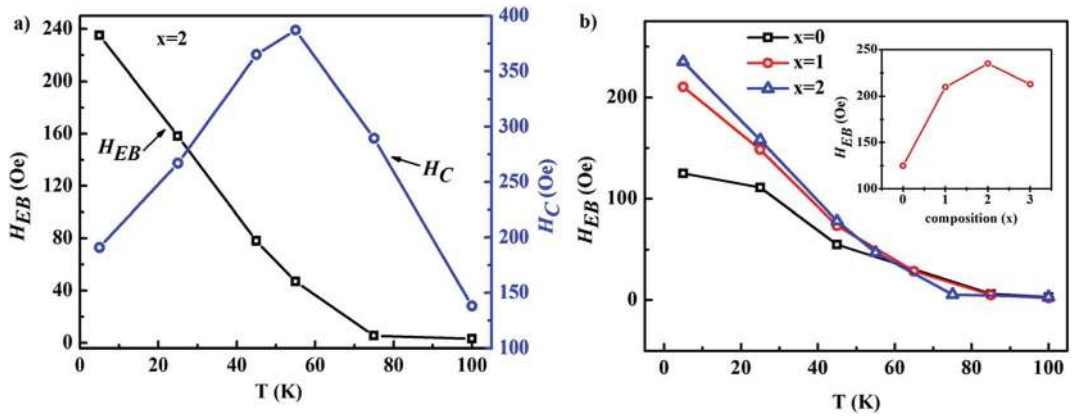

Fig. 10 H_{EB} and H_C *vs.* T for (a) $Ni_{50}Mn_{36}Sn_{12}Si_2$ after field cooling from 350 K in an applied field of 10 kOe. (b) H_{EB} for $x = 0$, 1 and 2 compositions at different temperatures in an applied field of 10 kOe. Inset in (b) shows the variation of H_{EB} for different compositions at 5 K.

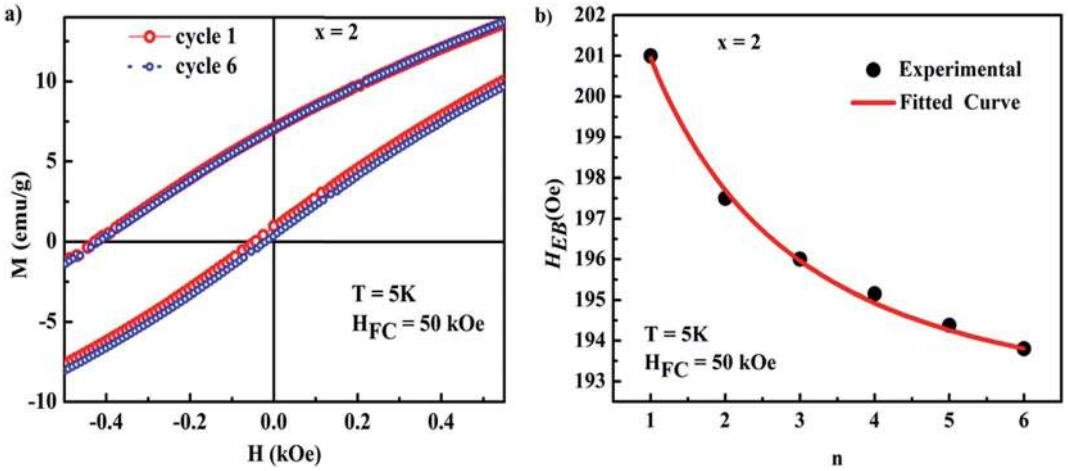

Fig. 12 (a) Training effect of exchange bias in $x = 2$. The first and sixth loops at 5 K are shown after field cooling in 50 kOe. (b) The dependence of H_{EB} on number of field cycles (n). The red solid line shows the best fit of eqn (1) to the experimental data.

However, a meticulous neutron diffraction study is essential to establish the above propositions concerning the magnetic state of these multifunctional alloys. From the present study it is clear that Si doping can tune the exchange bias property and it facilitates the search for new Heusler alloys with large exchange bias.

IV. Conclusions

The effect of Si substitution on the structure, magnetism and exchange bias properties of $Ni_{50}Mn_{36}Sn_{14-x}Si_x$ ($x = 0$, 1, 2 and 3) Heusler alloys has been investigated. The substitution of Si for Sn in these alloys results in a decrease in the lattice parameter due to the smaller ionic radius of Si. Strong frequency dependence of AC susceptibility clearly demonstrates the SG-like behavior close to the EB blocking temperature, above which EB effect vanishes. Enhanced exchange bias in Si substituted Ni–Mn–Sn Heusler alloys have been observed below their martensitic transition temperature and it arises due to the unidirectional anisotropy which is caused by the coupling between the ferromagnetic and spin glass like component in the martensitic phase. Exchange bias effect is found to increase with Si concentration initially and a value of 235 Oe is obtained for $x = 2$ alloy. The observation of training effect and double shifted hysteresis loops further confirm the exchange bias phenomenon in these materials. Therefore, the present results seem to be very promising in the search for multifunctional materials from the Heusler alloy family.

Acknowledgements

The authors acknowledge CSIR 12th Five Year Plan Project, "Sustainable technologies for the Utilization of Rare-earths (SURE)", (No. CSC0132) for financial support. G. R. Raji, Manoj Raama Varma and K. G. Suresh would like to acknowledge BRNS, Bombay for their financial support. G. R. Raji acknowledges the Department of Science and Technology, India for the financial support *via* the project DST No. SR/S3/ME/0019/2010. Bhagya Uthaman is thankful to KSCSTE (Kerala State Council for Science, Technology and Environment) for granting Junior Research Fellowship. Rajesh Kumar Rajan acknowledges Council of Scientific and Industrial Research (CSIR) for granting the fellowship. S. Thomas kindly acknowledges the financial support provided by the Department of Science and Technology, India, *via* the INSPIRE Faculty award. We also acknowledge Dr P. N. Santhosh, Professor, IIT Madras for the fruitful suggestions regarding the crystal structure. Special thanks to Mr Ajeesh. P. Paulose for his timely technical support.

References

1 W. H. Meiklejohn and C. P. Bean, *Phys. Rev.*, 1956, **102**, 1413.
2 J. Nogués and I. K. Schuller, *J. Magn. Magn. Mater.*, 1999, **192**, 203.
3 R. H. Kodama, A. E. Berkowitz, E. J. McNiff and S. Foner, *Phys. Rev. Lett.*, 1996, **77**, 394.
4 W. H. Meiklejohn, *J. Appl. Phys.*, 1962, **33**, 1328.
5 E. Arenholz, K. Liu, Z. P. Li and I. K. Schuller, *Appl. Phys. Lett.*, 2006, **88**, 072503.
6 M. Gruyters, *Phys. Rev. Lett.*, 2005, **95**, 077204.
7 Y. K. Tang, Y. Sun and Z. H. Cheng, *Phys. Rev. B: Condens. Matter Mater. Phys.*, 2006, **73**, 174419.
8 T. Qian, G. Li, T. Zhang, T. F. Zhou, X. Q. Xiang, X. W. Kang and X. G. Li, *Appl. Phys. Lett.*, 2007, **90**, 012503.
9 R. Kainuma, Y. Imano, W. Ito, Y. Sutou, H. Morito, S. Okamoto, O. Kitakami, K. Oikawa, A. Fujita, T. Kanomata and K. Ishida, *Nature*, 2006, **439**, 957.
10 V. K. Sharma, M. K. Chattopadhyay, K. H. B. Shaeb, A. Chouhan and S. B. Roy, *Appl. Phys. Lett.*, 2006, **89**, 222509.
11 S. Y. Yu, Z. H. Liu, G. D. Liu, J. L. Chen, Z. X. Cao, G. H. Wu, B. Zhang and X. X. Zhang, *Appl. Phys. Lett.*, 2006, **89**, 162503.
12 T. Krenke, E. Duman, M. Acet, E. F. Wassermann, X. Moya, L. Mañosa and A. Planes, *Nat. Mater.*, 2005, **4**, 450.

13 A. K. Pathak, M. Khan, I. Dubenko, S. Stadler and N. Ali, *Appl. Phys. Lett.*, 2007, **90**, 262504.
14 Z. Li, C. Jing, J. P. Chen, S. J. Yuan, S. X. Cao and J. C. Zhang, *Appl. Phys. Lett.*, 2007, **91**, 112505.
15 A. K. Nayak, K. G. Suresh and A. K. Nigam, *J. Phys. D: Appl. Phys.*, 2009, **42**, 115004.
16 G. R. Raji, U. Bhagya, S. Thomas, K. G. Suresh and M. R. Varma, *J. Appl. Phys.*, 2015, **117**, 103908.
17 J. Sharma and K. G. Suresh, *Appl. Phys. Lett.*, 2015, **106**, 072405.
18 A. K. Pathak, M. Khan, B. R. Gautam, S. Stadler, I. Dubenko and N. Ali, *J. Magn. Magn. Mater.*, 2009, **321**, 963.
19 H. C. Xuan, Q. Q. Cao, C. L. Zhang, S. C. Ma, S. Y. Chen, D. H. Wang and Y. W. Du, *Appl. Phys. Lett.*, 2010, **96**, 202502.
20 L. Ma, W. H. Wang, J. B. Lu, J. Q. Li, C. M. Zhen, D. L. Hou and G. H. Wu, *Appl. Phys. Lett.*, 2011, **99**, 182507.
21 A. K. Nayak, K. G. Suresh and A. K. Nigam, *J. Phys.: Condens. Matter*, 2011, **23**, 416004.
22 Z. Liu, Z. Wu, H. Yang, Y. Liu, W. Wang, X. Ma and G. Wu, *Intermetallics*, 2011, **19**, 1605.
23 V. V. Kokorin, I. A. Osipenko and T. V. Shirina, *Phys. Met. Metallogr.*, 1989, **67**, 173.
24 W. Ito, M. Nagasako, R. Y. Umetsu, R. Kainuma, T. Kanomata and K. Ishida, *Appl. Phys. Lett.*, 2008, **93**, 232503.
25 X. Jin, M. Marioni, D. Bono, S. M. Allen, R. C. O'Handley and T. Y. Hsu, *J. Appl. Phys.*, 2002, **2002**(91), 8222.
26 L. Manosa, X. Moya, A. Planes, O. Gutfleisch, J. Lyubina, M. Barrio, J. L. Tamarit, S. Aksoy, T. Krenke and M. Acet, *Appl. Phys. Lett.*, 2008, **92**, 012515.
27 J. X. Wu, B. H. Jiang and T. Y. Hsu, *Acta Metall.*, 1988, **36**, 1521.
28 S. Esakki Muthu, S. Singh, R. Thiyagarajan, G. Kalai Selvan, N. V. Rama Rao, M. Manivel Raja and S. Arumugam, *J. Phys. D: Appl. Phys.*, 2013, **46**, 205001.
29 S. Miyazaki and K. Otsuka, *ISIJ Int.*, 1989, **29**, 353.
30 S. H. Hai, Y. H. Jun, F. Hao, G. Y. Jun, F. Y. Qing and Z. X. Tao, *Chin. Phys. B*, 2011, **20**, 046102.
31 X. G. Zhao, C. C. Hsieh, W. C. Chang, W. Liu and Z. D. Zhang, *J. Phys.: Conf. Ser.*, 2011, **266**, 012128.
32 A. K. Pathak, I. Dubenko, S. Stadler and N. Ali, *J. Phys. D: Appl. Phys.*, 2008, **41**, 202004.
33 P. A. Bhobe, K. R. Priolkar and P. R. Sarode, *J. Phys.: Condens. Matter*, 2008, **20**, 015219.
34 L. Ma, W. H. Wang, J. B. Lu, J. Q. Li, C. M. Zhen, D. L. Hou and G. H. Wu, *Appl. Phys. Lett.*, 2011, **99**, 182507.
35 S. Chatterjee, S. Giri, S. K. De and S. Majumdar, *Phys. Rev. B: Condens. Matter Mater. Phys.*, 2010, **79**, 092410.
36 J. A. Mydosh, *Spin Glasses: An Experimental Introduction*, Taylor & Francis, London, 1993, p. 68.
37 Y. Sutou, Y. Imano, N. Koeda, T. Omori, R. Kainuma, K. Ishida and K. Oikawa, *Appl. Phys. Lett.*, 2004, **85**, 4358.
38 M. Khan, I. Dubenko, S. Stadler and N. Ali, *Appl. Phys. Lett.*, 2007, **91**, 072510.
39 A. K. Nayak, R. Sahoo, K. G. Suresh, A. K. Nigam, X. Chen and R. V. Ramanujan, *Appl. Phys. Lett.*, 2011, **98**, 232502.
40 S. Thomas, D. Nissen and M. Albrecht, *Appl. Phys. Lett.*, 2014, **105**, 022405.
41 S. Thomas, G. Pookat, S. S. Nair, M. Daniel, B. Dymerska, A. Liebig, S. H. Al-Harthi, R. V. Ramanujan, M. R. Anantharaman, R. J. Fidler and M. Albrecht, *J. Phys.: Condens. Matter*, 2012, **24**, 256004.
42 C. Binek, *Phys. Rev. B: Condens. Matter Mater. Phys.*, 2004, **70**, 014421.